ACS APPLIED MATERIALS & INTERFACES

www.acsami.org

Research Article

Dye-Loaded Quatsomes Exhibiting FRET as Nanoprobes for Bioimaging

Judit Morla-Folch, Guillem Vargas-Nadal, Tinghan Zhao, Cristina Sissa, Antonio Ardizzone, Siarhei Kurhuzenkau, Mariana Köber, Mehrun Uddin, Anna Painelli, Jaume Veciana, Kevin D. Belfield,* and Nora Ventosa*

Cite This: *ACS Appl. Mater. Interfaces* 2020, 12, 20253−20262

Read Online

ACCESS | Metrics & More | Article Recommendations | Supporting Information

ABSTRACT: Fluorescent organic nanoparticles (FONs) are emerging as an attractive alternative to the well-established fluorescent inorganic nanoparticles or small organic dyes. Their proper design allows one to obtain biocompatible probes with superior brightness and high photostability, although usually affected by low colloidal stability. Herein, we present a type of FONs with outstanding photophysical and physicochemical properties in-line with the stringent requirements for biomedical applications. These FONs are based on quatsome (QS) nanovesicles containing a pair of fluorescent carbocyanine molecules that give rise to Förster resonance energy transfer (FRET). Structural homogeneity, high brightness, photostability, and high FRET efficiency make these FONs a promising class of optical bioprobes. Loaded QSs have been used for in vitro bioimaging, demonstrating the nanovesicle membrane integrity after cell internalization, and the possibility to monitor the intracellular vesicle fate. Taken together, the proposed QSs loaded with a FRET pair constitute a promising platform for bioimaging and theranostics.

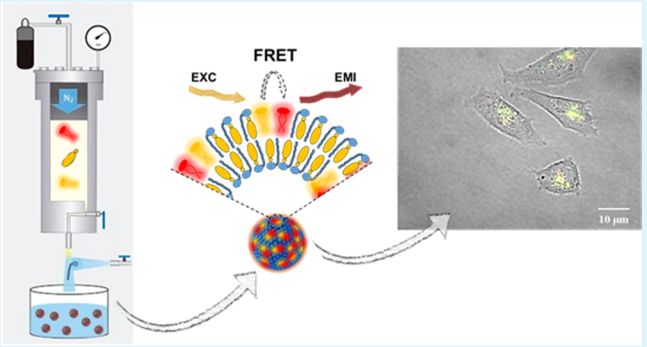

KEYWORDS: *bioimaging, fluorescent organic nanoparticles, FRET, quatsomes, bioprobes*

INTRODUCTION

Over the last few years, we have witnessed an upsurge of interest in the development of nanoparticles/nanovesicles exhibiting Förster or fluorescence resonance energy transfer (FRET) phenomenon for biosensing, bioimaging, and theranostic applications.[1−5] FRET occurs when a donor fluorophore in the excited state nonradiatively transfers energy to a nearby acceptor fluorophore (typically within a distance of 1−10 nm).[6,7] Loading a nanovesicle with a FRET pair rather than with a single fluorophore gives the possibility to monitor the integrity of the nanostructure in cell media, body fluids, or organs through FRET emission.[8] Additionally, FRET offers a wider spectral gap between the excitation and emission maxima than single fluorophores, thus significantly reducing self-absorption and, hence, the background noise while imaging. Moreover, FRET enables multiplex-imaging, where, upon exciting with a single light source, emission occurs in multiple spectral windows.[7] FRET assays based on organic dyes have the advantage of modest cost, simple preparation, and the possibility to use a variety of organic dyes that are convenient for diverse applications.[9] However, weak signal, low chemical stability, rapid fluorescence lifetime, and poor photobleaching resistance are continuous challenges for organic dye-based FRET assays.[4]

Nanoparticles (NPs) based on soft organic materials have recently gained considerable attention due to their ease of preparation/fabrication and promising flexibility in material synthesis with respect to the selection and combination of their constituents.[10,11] Several approaches to synthesize bright fluorescent organic nanoparticles (FONs) based on the direct assembly of dyes,[12] or exploiting nanovesicles and micelles have been reported.[13] Among nanovesicles, liposomes have been widely investigated as nanocarriers in the biomedical area. Constituted by at least one lipid bilayer with spherical shape, liposomes are biocompatible molecular self-assembled structures that can carry hydrophobic and hydrophilic molecules in biological media, representing one of the best platforms for drug-delivery and bioimaging.[14] However, their applicative potential is significantly reduced due to their aggregation tendency and their low on-shelf stability.[15,16] On the other

Received: February 20, 2020
Accepted: April 9, 2020
Published: April 9, 2020

https://dx.doi.org/10.1021/acsami.0c03040
ACS Appl. Mater. Interfaces 2020, 12, 20253−20262

hand, polymeric micelles are widely used carriers of FRET pairs of organic dyes, used not only as bioimaging probes[5,17−20] but also as reporters of the micelle's stability.[8,21] However, several shortcomings of current dye-loaded polymer nanoparticles (NPs) need to be addressed, including aggregation-caused quenching (ACQ),[12] surface chemistry, colloidal stability, and micelle dissociation induced by shear stress.[8]

To overcome these challenges, we use highly stable and monodisperse quatsome (QS) nanovesicles as carriers and integrate a FRET pair of amphiphilic carbocyanine dyes in the vesicle membrane. QSs are thermodynamically stable nanoscopic unilamellar vesicles, made by quaternary ammonium surfactants and sterols, such as CTAB and cholesterol in an equimolar ratio.[22,23] Molecular dynamic simulations have revealed that in the presence of water, CTAB and cholesterol molecules self-assemble first into bimolecular amphiphiles, followed by the formation of bilayers.[22] The structure of these bilayers is identical to those formed by double-tailed unimolecular amphiphiles. These kinds of nanostructures are highly homogeneous colloidal systems and can be functionalized with targeting ligands, such as peptides, for site-specific recognition. For instance, QS functionalized with cell-penetrating peptides has been achieved through their covalent conjugation to a fraction of cholesterol QS membrane components.[24] Due to their versatility, these nanovesicles have aroused considerable interest in biomedical applications.[25−27] QSs are used as nanocarriers to stabilize and transport organic dyes in aqueous media, while simultaneously enhancing their photostability and biocompatibility.[28] Moreover, high brightness is generally displayed due to the confinement of a large number of dye molecules in a small space, hence increasing their absorption coefficient.[5] What is more interesting for our aims is, however, the possibility offered by the nanoparticles to confine the FRET pair in a nanosized domain, opening a wide range of possibilities for molecular imaging and biosensing.

RESULTS AND DISCUSSION

Preparation of Dye-Loaded Quatsomes Exhibiting FRET. Here, we report QSs loaded with a FRET pair composed of the indocarbocyanine donor 1,1′-dioctadecyl-3,3,3′3′-tetramethylindocarbocyanine perchlorate (DiI) and the acceptor 1,1′-dioctadecyl-3,3,3′,3′-tetramethylindodicarbocyanine perchlorate (DiD) (see Figure S1). QSs loaded with DiI or DiD as well as simultaneously loaded with both dyes at an equimolar ratio[29] (QS-I, QS-D, and QS-I,D, respectively) (see Scheme 1) were prepared by a one-step method using the green technology referred to as depressurization of expanded liquid organic solution−suspension (DELOS-suspension) methodology.[24,30] The simultaneous loading of two different dyes did not affect the mean size of QSs (∼150 nm) or their morphology, as is evidenced by the cryo-transmission electron microscopy (TEM) images and by the nanoparticle tracking analysis (NTA) (Figure 1 and Table S1). As previously reported, QSs show a high vesicle-to-vesicle homogeneity in terms of morphology, size, and membrane lamellarity[22,28] in comparison to the majority of vesicular systems.[31] Despite the different lengths of the conjugated bridges of DiI and DiD, the inclusion in the QS membrane is very similar, leading to an ∼100 μM dye concentration in all samples. Thereby, thousands of molecules are successfully entrapped in a single QS, ensuring efficient FRET.

Scheme 1. Depiction of (a) Chemical Structure of the Carbocyanine Dyes and the Membrane Components, (b) Schematic Representations of Chol/CTAB QSs Loaded with Carbocyanine Dyes, DiI (yellow), and DiD (red), and (c) Cross-Sectional View of the QS-I,D Membrane

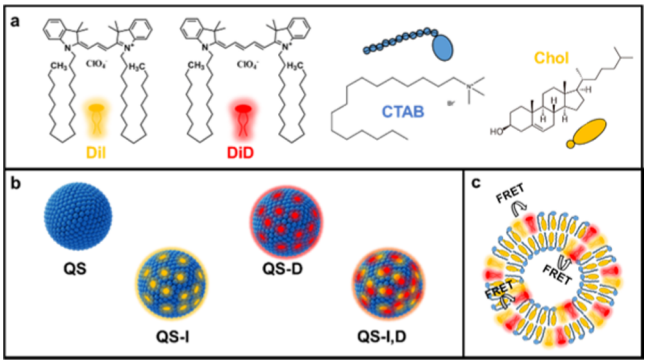

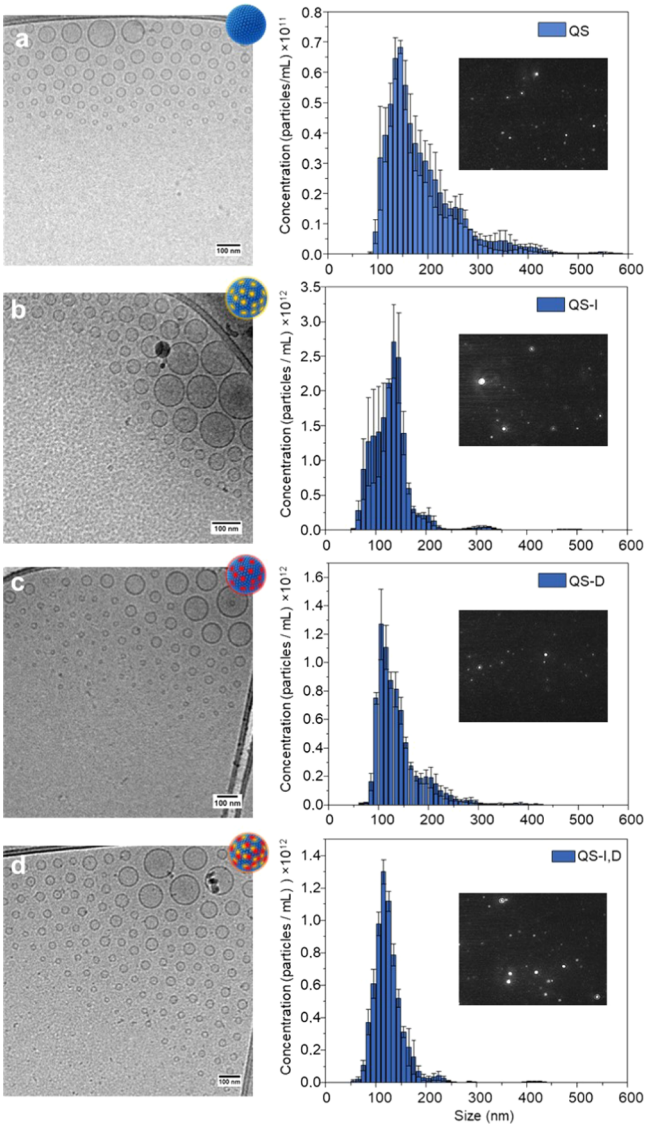

Figure 1. Cryo-TEM images (left) and size distribution profiles (right) measured by nanoparticle tracking analysis (NTA) of (a) plain QSs, (b) QSs loaded with DiI (QS-I), (c) QSs loaded with DiD (QS-D), and (d) QSs loaded with DiI and DiD (QS-I,D). Insets show screenshots from the NTA videos.

https://dx.doi.org/10.1021/acsami.0c03040
ACS Appl. Mater. Interfaces 2020, 12, 20253−20262

Table 1. Photophysical Properties of Dye-Loaded QSs

		λ_{max} abs[a] (nm)		λ_{max} emi[a] (nm)		$\Delta\nu$[b] (cm^{-1})		τ[c] (ns)		ϕ_F[d] (%)		brightness$_p$[e] ($\times 10^6$) M^{-1} cm^{-1}		ϕ_{Ph}[f] ($\times 10^{-6}$)		FRET efficiency[g] (%)
		DiI	DiD	DiI	DiD	DiI	DiD	DiI	DiD	DiI	DiD	DiI	DiD	DiI	DiD	
dyes in EtOH	DiI	552		570		572		0.40		10				0.05		
	DiD		649		674		572		1.31		37				5.8	
quatsomes in water	QS-I	552		570		572		0.78		18		77		7.5		
	QS-D		649		673		549		1.41		33		185		37.3	
	QS-I,D	552	649	569	673	3257		0.65	1.47	14	35	123 (for DiD)		3.73	22.3	85

[a]Absorption and emission maxima ±1 nm. [b]Stokes shift. [c]Fluorescence lifetimes ±5%. [d]Fluorescence quantum yield ±10%. [e]Brightness of a single fluorescent QS calculated as $\varepsilon_p \times \phi_F$, where ϕ_F is the fluorescence quantum yield and ε_p is the molar extinction coefficient at the maximum absorption wavelength of a single QS, calculated as $\varepsilon \times n$ (n is the estimated number of fluorophores per vesicle, see Table S2). [f]Photochemical decomposition quantum yields ±12%, λ_{ex} = 532 nm for DiI in ethanol, QS-I and QS-I,D in aqueous media, λ_{ex} = 650 nm for DiD in ethanol and QS-D in aqueous media. [g]FRET efficiency ±5%.

Photophysical Properties. The photophysical properties of DiI and DiD in ethanol and in dye-loaded QSs in water are summarized in Table 1. Steady-state absorption and excitation are presented in Figure 2. Absorption spectra of dye-loaded QSs in water compare well with the spectra of dyes in ethanol (dotted lines, Figure 2b), suggesting marginal aggregation phenomena, in contrast to the well-known tendency of cyanine dyes to aggregate.[32,33] The absorption maxima at ∼552 and ∼649 nm for QSs loaded with both dyes (Figure 2b) indicate the successful simultaneous loading of DiI and DiD in the DELOS-susp preparation. The minor intensity differences of the ∼600 nm shoulder in QSs may be ascribed to the presence of a minimal quantity of DiD H-aggregates, primarily H-dimers[34] (see Figure S2 for further analysis). In view of the marginal spectral differences observed, we safely assume that at L = 0.026 (loading = mg dye/mg membrane components), the stability of the dyes is not compromised in the QS membrane. The comparison between absorption and excitation spectra (Figure 2b) unambiguously demonstrates the occurrence of efficient FRET in QS-I,D, with a sizeable donor (DiI) contribution to the excitation spectrum when probing the acceptor (DiD) emission at λ_{em} = 710 nm. Indeed, QS-I,D were found to have high FRET efficiency (E_{FRET}). Upon excitation at 490 nm, two emission bands appeared at ∼569 and ∼673 nm corresponding to the DiI and DiD emission, respectively (Figure 2c). The fluorescence intensity of the donor dramatically decreased in the presence of the acceptor, resulting in an E_{FRET} of 85%. This value is significantly high in comparison to previous nanoparticles loaded with carbocyanine dyes exhibiting FRET.[8,17,20,21]

Time-resolved fluorescence measurements, exploiting the time-correlated single-photon counting (TCSPC) technique, further confirm efficient FRET (see Figure S3). The very short excited-state lifetime of the DiI in solution increases considerably when the dye is in the QS nanostructure. The donor lifetime decreases considerably when the acceptor (DiD) is also present in the same QS (see Figure 2d and Table 1). The short lifetime of DiI in ethanol may be assigned to the rapid relaxation of the excited state by cis−trans photoisomerization occurring at the polymethine linkage.[29] When the rotation about the polymethine linkage is prevented (by steric constraints, i.e, when the dye is located in the QS membrane), the fluorescence lifetimes become longer, as previously described elsewhere.[35] DiI average lifetime in the QS membrane is in agreement with the previously reported values in nanovesicles (i.e., 0.80 ns for DiI in the pure fluid-state lipid DOPC bilayer).[36] Similarly, the DiD lifetime increased when the dye was embedded in the QS membrane. It is important to note that DiI and DiD are not immobilized in the QS membrane but rather diffuse freely through the QS membrane with a diffusion coefficient that has a magnitude similar to that of phospholipid molecules in a lipid bilayer.[37]

Fluorescence quantum yields (ϕ_F) for dyes in ethanol and in the quatsome assemblies in water were also investigated. ϕ_F of DiI and DiD in ethanol changes from 10 and 37% in solution to 18 and 34% once located inside the QS membrane, respectively, confirming the more constrained environment of the QS membrane, as demonstrated previously by lifetime results. Since it is well known that the quantum yield is markedly dependent on viscosity,[7,35] complementary analysis varying the viscosity of the media were performed (Figure S4), demonstrating how the increase in viscosity results in increased ϕ_F and τ. Accordingly, quantum yields of 9 and >16% for free Cy3[38] and Cy3-DNA conjugates,[35] respectively, are reported in the literature. Our results (see Table 1) are in agreement with those reported for DiD in solution and entrapped in PLGA-PEG-maleimide polymer nanoparticles (ca. 60 nm) at ∼30[39,40] and 34%,[17] respectively.

Evaluation of Dye Leakage of the QS Membrane. Energy transfer typically occurs between dyes separated by 1−10 nm. Accordingly, since the QS membrane thickness is ca. 4 nm,[37] FRET is expected to occur not only between dyes located in the same vesicle leaflet but also between dyes located in different leaflets, as represented in Scheme 1c. To rule out FRET occurring between dyes on different QS, single dye-loaded QS (QS-I and QS-D) were mixed in aqueous media at equimolar concentration and FRET emission was then interrogated just after the sample preparation and 1 week later (Figure 3). As shown in Figure 3b, the excitation of DiI is negligible for emission at 710 nm. The emission spectra (Figure 3c) show a weak feature at 650−670 nm, which may indeed be related to a minor contribution from residual FRET (see Figure S5 for more detailed information). Therefore, we conclude that there is no significant contribution to FRET from dyes incorporated in different QSs. Moreover, we can safely conclude that there is no exchange of dyes between different QS vesicles. This is an important result; even if the dyes are not covalently linked to the QS membrane, the hydrophobic interaction is strong enough to stably constrain the fluorophores in the QS membrane.

https://dx.doi.org/10.1021/acsami.0c03040
ACS Appl. Mater. Interfaces 2020, 12, 20253−20262

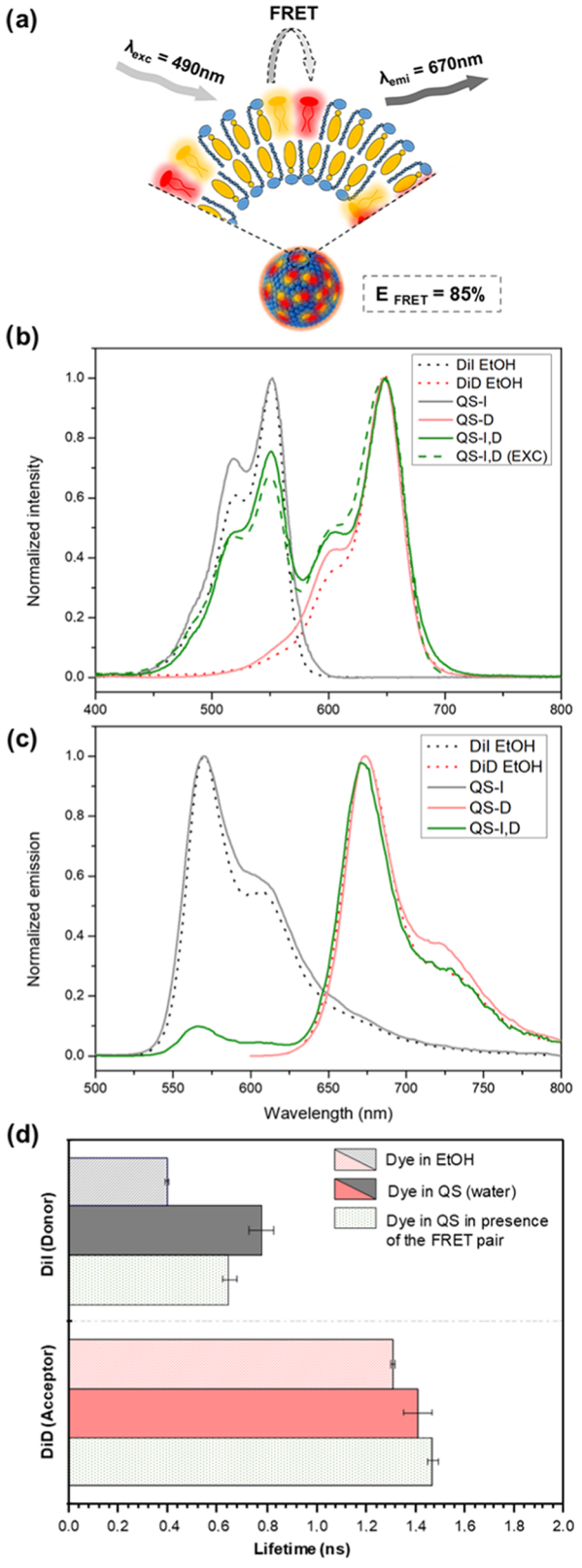

Figure 2. (a) Schematic representation of FRET in the QS membrane. (b) Normalized absorption spectra of dyes in ethanol and of the dye-loaded QSs in water, compared with the excitation spectra of QSs loaded with the FRET pair (QS-I,D, λ_{em} = 710 nm). (c) Normalized emission spectra of DiI and DiD in ethanol, QS-I, QS-D, and QS-I,D in water (λ_{ex} = 490 nm for DiI, QS-I, and QS-I,D; and λ_{ex} = 590 nm for DiD and QS-D) and, (d) representation of the lifetime values of dyes in ethanol and of the dye-loaded QSs in water.

Colloidal Stability, Brightness, and Photostability. Having optically characterized QS-I,D, we assessed their potential for bioimaging. An ideal fluorescent bioprobe for microscopy should be bright, stable over time, biocompatible, and photostable. In this regard, the stability, brightness, and photodegradation quantum yield (ϕ_{ph}) of the QSs exhibiting FRET were interrogated. Heretofore, the stability of dye-loaded QSs has been investigated via absorption measurements.[28] Since FRET emission only occurs when the D−A pair is within 1−10 nm, FRET emission and efficiency were monitored over time (Figure 4) showing no appreciable changes for at least 8 months, revealing the high degree of stability possessed by these dye-loaded nanocarriers. The absorption coefficients of individual carbocyanine-loaded QS (ε_p) (Table S2) and the theoretical brightness per particle (brightness$_p$) were also determined as they provide a more representative approximation of the brightness enhancement of the dye-loaded QSs compared to the single fluorophore molecules in solution. The QS-I,D possesses a high brightness of 1.2×10^8 M^{-1} cm^{-1} (see Table 1), which compares with the best results reported for the most common quantum dots[41] and dye-loaded polymeric nanoparticles,[5] typically in the range of 10^6−10^8 M^{-1} cm^{-1}.

Photostability is a stringent requirement for bioimaging applications due to the prolonged or reiterated irradiation of the probe.[42] Photodegradation studies (Figure S6) leads to important conclusions. First, the estimated photodegradation quantum yield, ϕ_{ph}, of the QS-D is ∼12 times less than DiD encapsulated in Pluronic micelles in water ($\phi_{ph} = 44 \times 10^{-5}$),[43] demonstrating a superior photostability of DiD entrapped in the QS membrane in comparison with micelles. This difference is likely due to the more rapid photodegradation of carbocyanine aggregates,[44] which are more abundant in micelles than in QSs. Second, the ϕ_{ph} of DiD in QS-I,D is of the same order of magnitude as in QS-D (see values in Table 1), even though the laser used for QS-I,D mainly excites DiI. These results confirm highly efficient energy transfer from DiI to DiD. For DiI, the same trends were observed, with DiI photostability increasing in the presence of the acceptor (QS-I,D), due to the altered kinetics of the donor's excited state in the presence of the acceptor.[45] Overall, the ϕ_{ph} obtained for the QS-I,D confirms their high photostability, suggesting their potential for bioimaging purposes.

Biocompatibility Tests and Cell Imaging. Cell viability tests and cell imaging studies were conducted for QS-I,D in commonly employed cancer and normal cell lines, specifically HeLa and CHO-K1, respectively. Figure 5 shows the cell viability after 24 h of incubation with several concentrations of QS-I,D, demonstrating low cytotoxicity for both cell lines up to a 5 μg/mL concentration. The cell viability with plain QS (no dye) and a CTAB surfactant in solution in HeLa cells (Figure 5b) provides evidence that the cytotoxicity is primarily due to the quaternary ammonium surfactant and is not significantly affected by the presence of dye, as has been reported for fluorenyl-loaded QS.[46] The effect of the cell membrane crossing on the integrity of the QS-I,D was analyzed by fluorescence imaging following the FRET emission. Based on the cell viability results, the cells were incubated with 0.5 μg/mL of QS-I,D for 2 h, providing bright images (see Figure S7 for comparison at higher concentrations). Figure 6a,b shows the fluorescence emission of QS-I,D at different wavelengths for HeLa and CHO-K1 cells, respectively. Importantly, FRET emission of QS-I,D and their colocalization with DiI emission

https://dx.doi.org/10.1021/acsami.0c03040
ACS Appl. Mater. Interfaces 2020, 12, 20253−20262

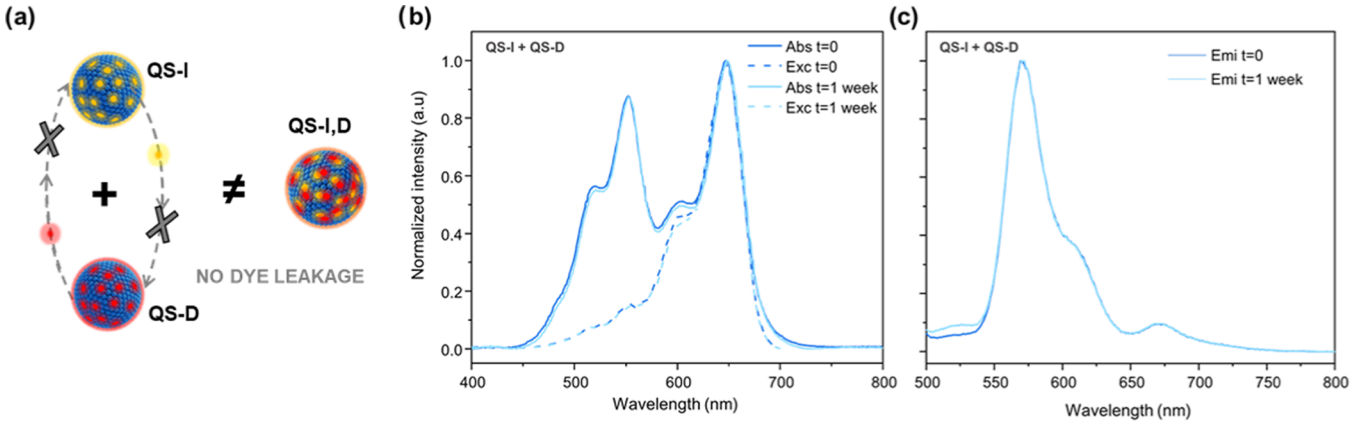

Figure 3. Analysis of the encapsulation stability and dye exchange between QSs. (a) Graphical representation of the dye leakage/exchange between distinct QSs in aqueous media, (b) normalized absorption and excitation spectra (λ_{em} = 710 nm), and (c) emission spectra (λ_{ex} = 490 nm) of a mixed solution of QS-I and QS-D (1:1) after sample preparation and 1 week later.

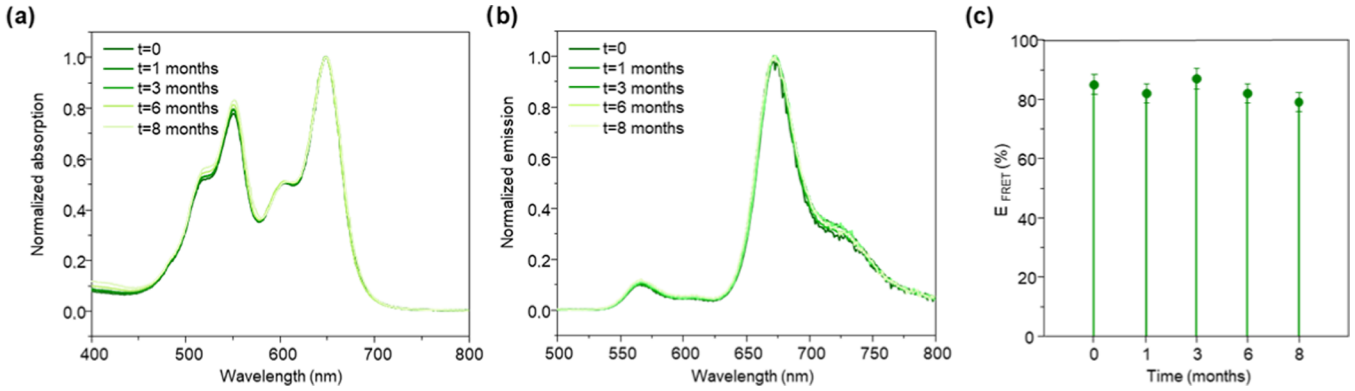

Figure 4. Stability of QS-I,D over time. (a) Absorbance spectra, (b) emission spectra, and (c) FRET efficiency representation of the QS-I,D after 1, 3, 6, and 8 months from the synthesis.

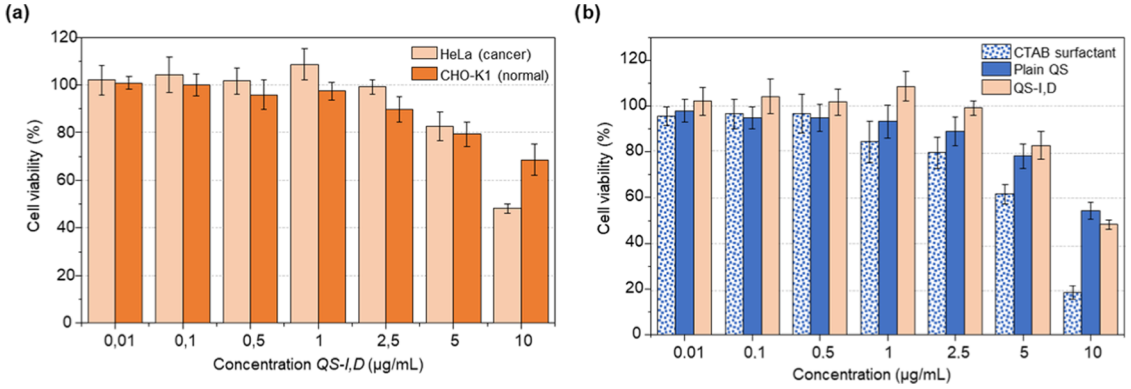

Figure 5. Cell viability assay of HeLa and CHO-K1 cells with (a) QS-I,D at various concentrations in HeLa and CHO-K1 cells and (b) CTAB surfactant dissolved in water, plain QSs (Chol/CTAB nanovesicles), and QSs loaded with DiI and DiD (QS-I,D) in HeLa cells, all solutions added in aqueous media at various concentrations.

manifest the integrity of the QS membrane inside the cells (both normal and cancer lines) and its stability at least for the considered time interval. These results confirm the good biocompatibility of QS-I,D and their capability of introducing specific organic fluorophores (and potentially, drugs) into the cell since the QS membrane integrity is ensured.

Cellular Colocalization Study. Finally, to elucidate the cellular distribution of QS-I,D, colocalization experiments were conducted using a commercial organelle marker. Based on previous results,[46] it is expected that QSs accumulate at the lysosome; hence, LysoTracker Green was employed to determine potential organelle selectivity. Fluorescence images collected for cells coincubated with LysoTracker Green and QS-I,D illustrate that their localization is highly coincident (Figure 6c,d). The Pearson's correlation coefficient was determined as 0.88 and 0.80 for HeLa and CHO-K1, respectively, indicating that lysosomes are the main organelle for QS localization in cells.

https://dx.doi.org/10.1021/acsami.0c03040
ACS Appl. Mater. Interfaces 2020, 12, 20253−20262

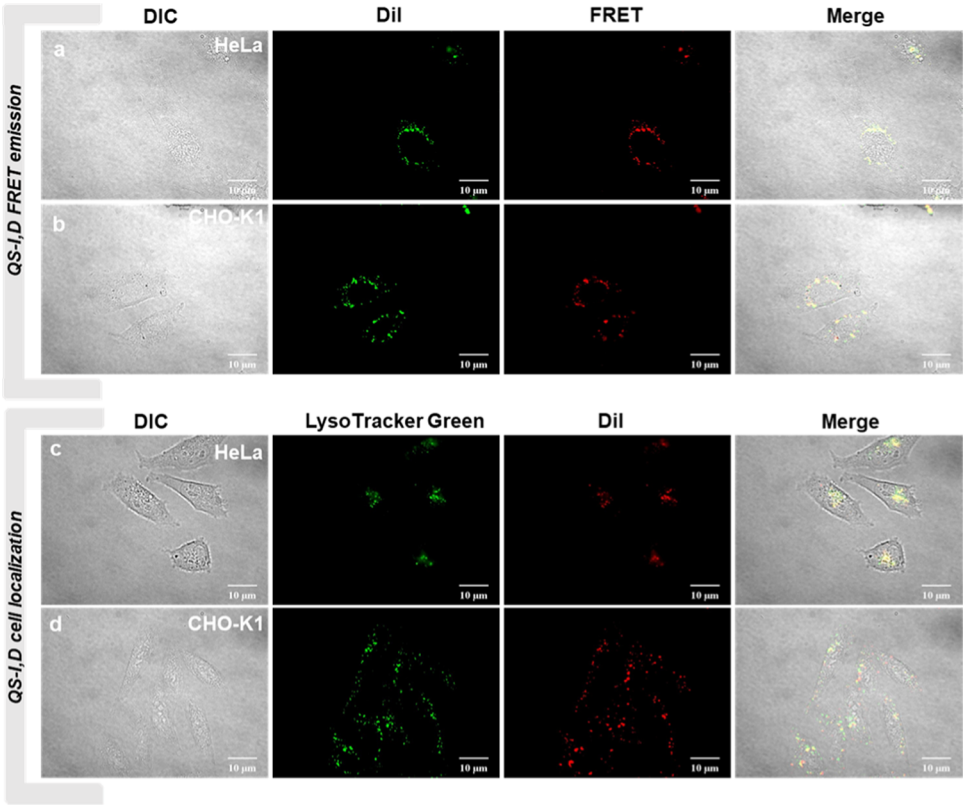

Figure 6. Fluorescence imaging. (a, b) FRET emission study in HeLa and CHO-K1 cells, respectively. Cells were incubated with 0.5 μg/mL of QS-I,D at 37 °C for 2 h. (c, d) Colocalization images of HeLa and CHO-K1, respectively. Cells were incubated with 0.5 μg/mL of QS-I,D for 2 h at 37 °C and 400 nM of LysoTracker Green was incubated with cells for 1 h before cell imaging. Cell imaging was performed by fluorescence microscopy, 60× oil immersion objective, Ex: 532/40; Em: 585/40—green channel and Ex: 482/40; Em: 624/40—red channel.

CONCLUSIONS

In summary, we have developed fluorescent organic nanoparticles showing efficient FRET based on the nanovesicles known as Quatsomes. Loading organic dyes into a nonfluorescent nanocarrier such as quatsomes offers an interesting strategy to improve their physicochemical and optical properties, overcoming most of the current challenges on the design of organic dye-based FRET assays. The obtained FONs allow the dispersion and stability of a FRET pair of organic dyes in aqueous media, ensuring long-term nanovesicle stability, high FRET efficiency, attractive spectroscopic properties, and biocompatibility. In particular, the fluorescent colloidal system is homogeneous in terms of size, morphology, and lamellarity and stable for at least 8 months, efficiently entrapping carbocyanine dyes without appreciable dye leakage. Moreover, the high brightness (123×10^6 vs 0.58×10^6 M^{-1} cm^{-1} for Qdot 605[47]) and low photodegradation quantum yield comparable to the commercially available fluorescent nanoparticles (ϕ_{ph} of QS-D is ~12 times lower than DiD in pluronic micelles), demonstrate the robustness of these nanovesicles. QSs exhibiting FRET are stable in cell media and maintain their integrity inside the cells, where they mainly localize in lysosomes. Considering the capability of these nanostructures to be easily functionalized and engineered with targeting units,[24] we anticipate that the described QSs loaded with FRET pairs are particularly interesting candidates for the development of fluorescent probes for the detection of specific biomarkers by bioimaging (in vitro and in vivo) and by medical diagnostic kits.

EXPERIMENTAL SECTION

Synthesis of FRET Pair-Loaded QS. *Preparation of Dye-Loaded Chol/CTAB QSs by DELOS-susp.* Plain and labeled QSs with DiI and/or DiD were prepared using the DELOS-susp (depressurization of an expanded liquid organic solution−suspension) method. This method has been previously described[24] and includes the depressurization of a CO_2-expanded organic liquid solution into an aqueous phase containing a solution or dispersion of a polar compound using mild conditions of temperature (308 K) and pressure (10 MPa). In a typical plain-quatsome preparation, 79.91 mg of cholesterol was added to 3.11 mL of ethanol, and then supercritical CO_2 was added, reaching one-phase in the reactor (7.3 mL of volume) containing the three components. After 1 h, the solution was depressurized over a solution of 72.56 mg of CTAB suspended in 25.11 mL of water. For the preparation of the labeled QSs with DiI and/or DiD, a solution of each dye in ethanol was added in the organic phase of the reactor, yielding a 100 μM of total dye in each preparation. Finally, the resulting suspension had a total concentration of plain and labeled QSs of 5.3 mg/mL. To remove the ethanol and the residual membrane components in the QS membrane, one step of purification was applied. In this study, we purified the as-prepared nanovesicles by diafiltration, using the KrosFlo Diafiltration equipment, from Spectrum Labs. In our case, we used a size-exclusion column of 100 kDa and a surface area of 20 cm^2 (MicroKros, Spectrum Labs). All of the quatsomes were diafiltered in Milli-Q water.

Determination of Dye Concentration and Loading in Dye-Loaded QSs. To determine the concentration and mass of dye entrapped in the QSs, the UV−vis absorbance of each dye was measured using a UV−vis spectrophotometer (Varian Cary 5, Agilent). The QS membrane was dissociated by diluting the samples in ethanol until a value of absorption unit of 0.1−0.3 is obtained. The concentration of each dye was determined using the Lambert−Beer

https://dx.doi.org/10.1021/acsami.0c03040
ACS Appl. Mater. Interfaces 2020, 12, 20253−20262

law (Abs = $c \times \varepsilon \times l$), where c is the concentration (M), ε is the molar extinction coefficient (M^{-1} cm^{-1}), and l is the path length (cm), using $\varepsilon^{DiI}_{550nm}$, EtOH = 140 000 M^{-1} cm^{-1}, $\varepsilon^{DiD}_{646nm}$, EtOH = 246 000 M^{-1} cm^{-1}, and a high precision cell (Hellma Analytics) of a 1 cm as a cuvette. For the determination of the loading, QSs were freeze-dried (LyoQuest-80, Telstar) at 193 K and 5 Pa for 1 week. Then, the freeze-dried dye-loaded QSs were weighted, and through eq 1, the loading in mass was determined.

$$\text{dye loading} = \frac{\text{mass of dye}}{\text{mass weighted} - \text{mass of dye}} \tag{1}$$

Physicochemical Characterization of Dye-Loaded QSs. *Nanoparticle Tracking Analysis (NTA).* Mean size and size distribution of QS, QS-I, QS-D, and QS-I,D were analyzed by NTA using a Nanosight NS300 (Malvern Instruments) equipped with a laser at 488 nm. The laser beam passes through the sample chamber, where particles in suspension scatter the light beam and can be easily visualized using a 20× magnification microscope equipped with a sCMOS camera (30 fps). The video captures the particle movements under Brownian motion, and using the Stokes−Einstein equation, the software determines the hydrodynamic diameter of the nanoparticles. The analysis was carried out at room temperature. Samples were diluted 10 000 times to fit the concentration range suggested by the manufacturer. The reported values are obtained as averages of results from five videos for each sample.

Cryo-TEM. Cryogenic transmission electronic microscopy (cryo-TEM) images were acquired with a JEOL JEM microscope (JEOL JEM 2011, Tokyo, Japan) operating at 200 kV under low-dose conditions. The sample was deposited onto the holey carbon grid and then was immediately vitrified by rapid immersion in liquid ethane. The vitrified sample was mounted on a cryo-transfer system (Gatan 626) and introduced into the microscope. Images were recorded on a CCD camera (Gatan Ultrascan US1000) and analyzed with the Digital Micrograph 1.8 software.

Electrophoretic Light Scattering (ELS). ζ-Potential measurements were performed with a Zetasizer Nano ZS (Malvern Instruments) using an incident light of 633 nm and measuring the scattered light at 13°. A DTS1070 folded capillary cell (Malvern Instruments) was used, applying a voltage of 40 mV between the electrodes. The measurements were performed without dilution at 298 K and Smoluchowski equation was employed. To ensure the reliability of the results, three different experiments were performed for each sample. This measurement could only be performed in the plain QS and QS-I samples. The determination of the ζ-potential cannot be done in the samples that contain DiD since this dye absorbs the 633 nm incident light. For this reason, the size measurements were performed with an NTA technique instead of DLS.

Photophysical Properties. *Steady-State Spectroscopy.* Steady-state absorption spectra were measured with a Tecan Infinite M200 PRO plate reader spectrometer in a 1 cm path length quartz cuvette. An FLS980 fluorescence spectrometer (Edinburgh Instruments) was employed for the recording of fluorescence emission and excitation spectra. The fluorescence spectra were corrected for the spectral responsivity of the detector. Diluted solutions were used for fluorescence measurements, with optical densities of ∼0.1.

Time-Resolved Spectroscopy. Time-resolved fluorescence intensity measurements were performed by time-correlated single-photon counting (TCSPC), using an Edinburgh Instrument FLS980 spectrofluorometer. Fluorescence decay curves were recorded on a time scale of 20 ns, resolved into 4096 channels, to a total of 10000 counts in the peak channel. DiI, QS-I, and QS-I,D were excited with a 509 nm laser (recording emission at 570 nm) and DiD and QS-D with a 635 nm laser (recording emission at 670 nm). Decay curves were analyzed using a standard iterative reconvolution method in the FLS980 software package, on the basis of the biexponential decay function. The quality of the fit was judged on the basis of the reduced χ^2 statistic, and the randomness of residuals.

Quantum Yield. The fluorescence quantum yield (ϕ_F) of QS-I and QS-D was determined following two methodologies. Based on the comparative method,[7,48] the values were calculated according to eq 2, using rhodamine B in water (ϕ_{ref} = 0.31) and cresyl violet in methanol (ϕ_{ref} = 0.54) as standards for DiI and DiD (in ethanol), respectively.

$$\phi_F = \phi_{ref}\frac{I}{I_r}\frac{OD_r}{OD}\frac{n^2}{n_r^2} \tag{2}$$

where ϕ_F is the quantum yield, I is the integrated fluorescence emission, OD is the optical density at the excitation wavelength, and n is the solvent refractive index of the sample, while I_r, OD_r, and n_r are the same parameters of the reference used.

The quantum yield of QS-I,D was estimated using another approach based on the ratio of the measured (τ) and natural lifetime (τ_n) (eq 3) because of the partial overlapping between the reference of the donor with the DiD. The natural lifetime was estimated accordingly to eq 4, where τ_n is natural or intrinsic lifetime, ϕ_F is the quantum yield, and Γ is the radiative decay rate, which can be calculated using the Strickler−Berg equation[49] (eq 5),

$$\tau_n = \frac{\tau}{\phi_F} \tag{3}$$

$$\tau_n = \frac{1}{\Gamma} \tag{4}$$

$$\Gamma = 2.88 \times 10^9\, n^2 \frac{\int F(\bar{\nu})\, d\bar{\nu}}{\int \frac{F(\bar{\nu})\, d\bar{\nu}}{\bar{\nu}^3}} \int \frac{\varepsilon(\bar{\nu})}{\bar{\nu}}\, d\bar{\nu} \tag{5}$$

where $F(\bar{\nu})$ is the emission spectrum plotted on the wavenumber (cm^{-1}) scale, $\varepsilon(\bar{\nu})$) is the absorption spectrum, and n is the refractive index of the medium. The integrals were calculated over the S0−S1 absorption and emission spectra. It is convenient to write this equation in terms of the more common units where the frequency is measured in cm^{-1} rather than s^{-1}. The ϕ_F of QS-I and QS-D measured following the two methodologies lead to consistent values within ±2%.

Photodegradation Quantum Yield. The quantum yields of the photoreactions, Φ_{ph}, were measured using the absorption method proposed by Belfield and Bondar,[50,51] determined from the temporal dependencies of the optical density at the maximum of the absorption band, $D(\lambda_{max}, t)$. The values $D(\lambda_{max}, t)$ were measured during irradiation with a laser for DiI, irradiation intensity: 8.15 mW/cm^2, excitation wavelength $\lambda_{exc} \approx$ 532 nm, and for DiD, irradiation intensity: 11 mW/cm^2, excitation wavelength $\lambda_{exc} \approx$ 650 nm. The intensity of the laser was measured with an IL-1400A power meter (International Light Inc.). The quantum yield of the photochemical reactions under one-photon excitation was calculated using eq 6.

$$\phi_{ph} = \frac{[D(\lambda, 0) - D(\lambda, t_{ir})]N_A}{10^3 \varepsilon(\lambda) \int_\lambda \int_0^{t_{ir}} I_0(\lambda)[1 - 10^{-D(\lambda, t)}]d\lambda\, dt} \tag{6}$$

where $D(\lambda, 0)$, $D(\lambda, t_{ir})$, $\varepsilon(\lambda)$, t, and λ are the initial and final optical density of the solution, extinction coefficient (M^{-1} cm^{-1}), irradiation time (s), and excitation wavelength (cm), respectively; N_A is the Avogadro's number; t_{ir} is the total irradiation time; and $I_0(\lambda)$ is the spectral distribution of the excitation irradiance.

FRET Efficiency. The efficiency of energy transfer (E_{FRET}) is the fraction of photons absorbed by the donor, which are transferred to the acceptor. It can be measured using different approaches, i.e., the relative fluorescence intensity of the donor, in the absence and presence of the acceptor, or from the calculated lifetime under these respective conditions. However, it is important to note that using these equations, it is assumed that the donor and the acceptor are separated by a fixed distance.[7] Considering that in the QS system dyes diffuse through the membrane, another approach was considered. The rate of energy transfer was then determined compared to the absorption spectrum and the excitation spectrum (eq 7) (through the observation of the acceptor fluorescence).[52]

https://dx.doi.org/10.1021/acsami.0c03040
ACS Appl. Mater. Interfaces 2020, 12, 20253−20262

$$E_{FRET} = \frac{A_A(\lambda_A)}{A_D(\lambda_D)}\left[\frac{I_A(\lambda_D, \lambda_A^{em})}{I_A(\lambda_A, \lambda_A^{em})} - \frac{A_A(\lambda_D)}{A_A(\lambda_A)}\right] \quad (7)$$

Biological Assays. *Cell Culture.* The HeLa line was selected as a cancer cell line (Cervical Adenocarcinoma, Human) and CHO-K1 as a normal line (Ovary, Chinese Hamster). These cell lines were selected because both come from the same organ (ovary). The HeLa cell line was cultured in Dulbecco's modified Eagle's medium (DMEM) supplemented with 10% fetal bovine serum, 1% penicillin/streptomycin at 37 °C in a humidified 5% CO_2 incubator. The CHO-K1 cell line was cultured in the Roswell Park Memorial Institute (RPMI) 1640 medium supplemented with 10% fetal bovine serum and 1% penicillin/streptomycin under the same conditions.

Cell Viability. To assess the cytotoxicity of QS-I,D, HeLa cells and CHO-K1 cells were cultured in the DMEM cell medium and RPMI 1640 cell medium, respectively, supplemented with 10% fetal bovine serum, 1% penicillin, and streptomycin at 37 °C and 5% CO_2. The cells were cultured in 96-well plates and incubated until 5×10^3 cells per well were quantified. Next, nanovesicles were added to the cells and incubated for an additional 22 h. QS-I,D were added at different concentrations (0.01, 0.1, 0.5, 1, 2.5, 5, and 10 μg/mL) where the values within parentheses refer to the nominal concentrations of the membrane components. Thereafter, 20 μL of the Cell Titer 96 Aqueous One solution reagent (for MTS assay) was added into each well, followed by further incubation for 2 h at 37 °C. The respective absorbance intensity at 490 nm were read on a Tecan Infinite M200 PRO plate reader spectrometer. Cell viabilities were calculated on the basis of eq 8, where Abs^{s}_{490nm} is the absorbance of the cells incubated with different concentrations of QS-I,D solutions, Abs^{D}_{490nm} is the absorbance of a cell-free well containing only QS-I,D at the concentration that was studied, Abs^{c}_{490nm} is the absorbance of cells incubated in the medium (without QS-I,D), and Abs^{D2}_{490nm} is the absorbance of the cell-free well.

$$\text{cell viability (\%)} = \frac{Abs^{s}_{490nm} - Abs^{D}_{490nm}}{Abs^{c}_{490nm} - Abs^{D2}_{490nm}} \times 100\% \quad (8)$$

Cellular Uptake and FRET Imaging Study. To investigate the cellular uptake of QS-I,D, HeLa cells and CHO-K1 cells were employed. All cells were seeded on a confocal dish (MatTek) at the density of 4×10^4 cells per dish and incubated for 24 h at 37 °C. QS-I,D was diluted to 0.5 and 1 μg/mL and with the DMEM cell medium, respectively, and freshly placed over cells for 2 h incubation period separately. The cells were washed three times with phosphate-buffered saline (PBS), and the live cell imaging solution (Molecular Probes) was added to confocal dishes. Fluorescence images were obtained using an inverted Olympus IX70 microscope coupled with a TRITC filter cube (Ex: 532/40; Em: 585/40) for DiI and a customized filter cube (Ex: 482/40; Em: 624/40) for FRET. Bright field, DiI field, and FRET field were obtained and issued by Fiji, freely available image processing software.

Cellular Colocalization Study. To investigate the efficiency and specificity of QS-I,D, HeLa and CHO-K1 cells were employed. All cells were seeded on a confocal dish (MatTek) at the density of 4×10^4 cells per dish and incubated for 24 h at 37 °C. QS-I,D was diluted in 0.5 μg/mL with the DMEM, respectively, and freshly placed over cells for a 2 h incubation period. The cells were washed three times with PBS, and the live cell imaging solution (Molecular Probes) was added to confocal dishes. LysoTracker Green (LT Green) (400 nM) was added 1 h before cell imaging. Fluorescence images were obtained using an inverted Olympus IX70 microscope coupled with a FITC filter cube (Ex: 482/40; Em: 534/40) for LT Green and a TRITC filter cube (Ex: 532/40; Em: 585/40) for DiI. Pearson's correlation coefficients for LT Green and DiI were calculated using Fiji software.

■ ASSOCIATED CONTENT

Supporting Information

The Supporting Information is available free of charge at https://pubs.acs.org/doi/10.1021/acsami.0c03040.

Normalized absorption and emission spectra of DiI and DiD in ethanol (Figure S1); physicochemical properties of Chol/CTAB QSs loaded with DiI and DiD (Table S1); absorption spectra of the experimental and calculated QSs loaded with DiI and DiD at 100 μM and 200 μM (Figure S2); time-resolved lifetime decay (Figure S3); study of the effect of viscosity on the ϕ_F and lifetime of DiI dye (Figure S4); dyes in solution (Figure S5); comparison of the dye brightness and per QS (Table S2); photochemical decomposition study (Figure S6); fluorescence images of HeLa and CHO-K1 cells incubated at different QS-I,D concentrations (Figure S7) (PDF)

■ AUTHOR INFORMATION

Corresponding Authors

Kevin D. Belfield − *Department of Chemistry and Environmental Science, College of Science and Liberal Arts, New Jersey Institute of Technology, Newark, New Jersey 07102, United States;* orcid.org/0000-0002-7339-2813; Email: belfield@njit.edu

Nora Ventosa − *Institut Ciencia dels Materials de Barcelona (ICMAB-CSIC), Campus UAB, 08193 Cerdanyola, Spain; Centro de Investigación Biomédica en Red CIBER-BBN, Barcelona, Spain;* orcid.org/0000-0002-8008-4974; Email: ventosa@icmab.es

Authors

Judit Morla-Folch − *Institut Ciencia dels Materials de Barcelona (ICMAB-CSIC), Campus UAB, 08193 Cerdanyola, Spain; Department of Chemistry and Environmental Science, College of Science and Liberal Arts, New Jersey Institute of Technology, Newark, New Jersey 07102, United States;* orcid.org/0000-0003-1059-6939

Guillem Vargas-Nadal − *Institut Ciencia dels Materials de Barcelona (ICMAB-CSIC), Campus UAB, 08193 Cerdanyola, Spain*

Tinghan Zhao − *Department of Chemistry and Environmental Science, College of Science and Liberal Arts, New Jersey Institute of Technology, Newark, New Jersey 07102, United States*

Cristina Sissa − *Dipartimento di Scienze Chimiche, della Vita e della Sostenibilità Ambientale, Università di Parma, 43124 Parma, Italy;* orcid.org/0000-0003-1972-1281

Antonio Ardizzone − *Institut Ciencia dels Materials de Barcelona (ICMAB-CSIC), Campus UAB, 08193 Cerdanyola, Spain*

Siarhei Kurhuzenkau − *Dipartimento di Scienze Chimiche, della Vita e della Sostenibilità Ambientale, Università di Parma, 43124 Parma, Italy*

Mariana Köber − *Institut Ciencia dels Materials de Barcelona (ICMAB-CSIC), Campus UAB, 08193 Cerdanyola, Spain; Centro de Investigación Biomédica en Red CIBER-BBN, Barcelona, Spain*

Mehrun Uddin − *Department of Chemistry and Environmental Science, College of Science and Liberal Arts, New Jersey Institute of Technology, Newark, New Jersey 07102, United States*

Anna Painelli − *Dipartimento di Scienze Chimiche, della Vita e della Sostenibilità Ambientale, Università di Parma, 43124 Parma, Italy;* orcid.org/0000-0002-3500-3848

Jaume Veciana − *Institut Ciencia dels Materials de Barcelona (ICMAB-CSIC), Campus UAB, 08193 Cerdanyola, Spain; Centro de Investigación Biomédica en Red CIBER-BBN, Barcelona, Spain;* orcid.org/0000-0003-1023-9923

https://dx.doi.org/10.1021/acsami.0c03040
ACS Appl. Mater. Interfaces 2020, 12, 20253−20262

Complete contact information is available at:
https://pubs.acs.org/10.1021/acsami.0c03040

Author Contributions

This manuscript was written through contributions of all authors. All authors have given approval to the final version of the manuscript.

Notes

The authors declare no competing financial interest.

■ ACKNOWLEDGMENTS

J.M.F. gratefully thank the financial support received by the European Union's Horizon 2020 research and innovation program under the Marie Skłodowska-Curie grant agreement no. 712949 (TECNIOspring PLUS) and from the Agency for Business Competitiveness of the Government of Catalonia (TECSPR17-1-0035). This work was also financially supported by the Ministry of Economy, Industry, and Competitiveness, Spain, through the "MOTHER" project (MAT2016-80826-R) and the "FLOWERS" project (FUNMAT-FIP-2016) funded by the Severo Ochoa (SEV-2015-0496) awarded to ICMAB. Instituto de Salud Carlos III, through "Acciones CIBER", also supported this work. Characterization of nanovesicles was made at the ICTS "NANBIOSIS", more specifically by the U6 unit of CIBER-BBN. The authors acknowledge the European Commission (EC) FP7-PEOPLE-2013-Initial Training Networks (ITN) "NANO2FUN" project no. 607721 for being the spark that initiated this work. K.B.D. acknowledges support from the National Science Foundation (CBET-1517273 and CHE-1726345). C.S. and A.P. benefited from the equipment and framework of the COMP-HUB Initiative, funded by the "Departments of Excellence" program of the Italian Ministry for Education, University and Research (MIUR, 2018-2022).

■ REFERENCES

(1) Algar, W. R.; Hildebrandt, N.; Vogel, S. S.; Medintz, I. L. FRET as a Biomolecular Research Tool — Understanding Its Potential While Avoiding Pitfalls. *Nat. Methods* **2019**, *16*, 815−829.
(2) Shi, J.; Tian, F.; Lyu, J.; Yang, M. Nanoparticle Based Fluorescence Resonance Energy Transfer (FRET) for Biosensing Applications. *J. Mater. Chem. B* **2015**, *3*, 6989−7005.
(3) Jares-Erijman, E. A.; Jovin, T. M. FRET Imaging. *Nat. Biotechnol.* **2003**, *21*, 1387.
(4) Shi, J.; Tian, F.; Lyu, J.; Yang, M. Nanoparticle Based Fluorescence Resonance Energy Transfer (FRET) for Biosensing Applications. *J. Mater. Chem. B* **2015**, *3*, 6989−7005.
(5) Reisch, A.; S, K. A. Fluorescent Polymer Nanoparticles Based on Dyes: Seeking Brighter Tools for Bioimaging. *Small* **2016**, *12*, 1968−1992.
(6) Förster, Th. Zwischenmolekulare Energiewanderung Und Fluoreszenz. *Ann. Phys.* **1948**, *437*, 55−75.
(7) Lakowicz, J. R. *Principles of Fluorescence Spectroscopy*, 2nd ed.; Kluwer Academic/Plenum: New York, 1999.
(8) Sun, X.; Wang, G.; Zhang, H.; Hu, S.; Liu, X.; Tang, J.; Shen, Y. The Blood Clearance Kinetics and Pathway of Polymeric Micelles in Cancer Drug Delivery. *ACS Nano* **2018**, *12*, 6179−6192.
(9) Terai, T.; Nagano, T. Fluorescent Probes for Bioimaging Applications. *Curr. Opin. Chem. Biol.* **2008**, *12*, 515−521.
(10) Aliprandi, A.; Mauro, M.; De Cola, L. Controlling and Imaging Biomimetic Self-Assembly. *Nat. Chem.* **2016**, *8*, 10−15.
(11) Tang, J.; Kong, B.; Wu, H.; Xu, M.; Wang, Y.; Wang, Y.; Zhao, D.; Zheng, G. Carbon Nanodots Featuring Efficient FRET for Real-Time Monitoring of Drug Delivery and Two-Photon Imaging. *Adv. Mater.* **2013**, *25*, 6569−6574.
(12) Kaeser, A.; Schenning, A. P. H. J. Fluorescent Nanoparticles Based on Self-Assembled π-Conjugated Systems. *Adv. Mater.* **2010**, *22*, 2985−2997.
(13) Jenkins, R.; Burdette, M. K.; Foulger, S. H. Mini-Review: Fluorescence Imaging in Cancer Cells Using Dye-Doped Nanoparticles. *RSC Adv.* **2016**, *6*, 65459−65474.
(14) Puri, A.; Loomis, K.; Smith, B.; Lee, J.-H.; Yavlovich, A.; Heldman, E.; Blumenthal, R. Lipid-Based Nanoparticles as Pharmaceutical Drug Carriers: From Concepts to Clinic. *Crit. Rev. Ther. Drug Carrier Syst.* **2009**, *26*, 523−580.
(15) Riehemann, K.; Schneider, S. W.; Luger, T. A.; Godin, B.; Ferrari, M.; Fuchs, H. Nanomedicine—Challenge and Perspectives. *Angew. Chem., Int. Ed.* **2009**, *48*, 872−897.
(16) Sercombe, L.; Veerati, T.; Moheimani, F.; Wu, S. Y.; Sood, A. K.; Hua, S. Advances and Challenges of Liposome Assisted Drug Delivery. *Front. Pharmacol.* **2015**, *6*, 286.
(17) Wagh, A.; Faidat, J.; Sanku, M.; Steven, Q.; Estelle, L.; Benedict, L. Polymeric Nanoparticles with Sequential and Multiple FRET Cascade Mechanisms for Multicolor and Multiplexed Imaging. *Small* **2013**, *9*, 2129−2139.
(18) Sun, G.; Berezin, M. Y.; Fan, J.; Lee, H.; Ma, J.; Zhang, K.; Wooley, K. L.; Achilefu, S. Bright Fluorescent Nanoparticles for Developing Potential Optical Imaging Contrast Agents. *Nanoscale* **2010**, *2*, 548−558.
(19) Chen, J.; Zhang, P.; Fang, G.; Yi, P.; Zeng, F.; Wu, S. Design and Synthesis of FRET-Mediated Multicolor and Photoswitchable Fluorescent Polymer Nanoparticles with Tunable Emission Properties. *J. Phys. Chem. B* **2012**, *116*, 4354−4362.
(20) Wagh, A.; Qian, S. Y.; Law, B. Development of Biocompatible Polymeric Nanoparticles for in Vivo NIR and FRET Imaging. *Bioconjugate Chem.* **2012**, *23*, 981−992.
(21) Morton, S. W.; Zhao, X.; Quadir, M. A.; Hammond, P. T. FRET-Enabled Biological Characterization of Polymeric Micelles. *Biomaterials* **2014**, *35*, 3489−3496.
(22) Ferrer-Tasies, L.; Moreno-Calvo, E.; Cano-Sarabia, M.; Aguilella-Arzo, M.; Angelova, A.; Lesieur, S.; Ricart, S.; Faraudo, J.; Ventosa, N.; Veciana, J. Quatsomes: Vesicles Formed by Self-Assembly of Sterols and Quaternary Ammonium Surfactants. *Langmuir* **2013**, *29*, 6519−6528.
(23) Grimaldi, N.; Andrade, F.; Segovia, N.; Ferrer-Tasies, L.; Sala, S.; Veciana, J.; Ventosa, N. Lipid-Based Nanovesicles for Nanomedicine. *Chem. Soc. Rev.* **2016**, *45*, 6520−6545.
(24) Cabrera, I.; Elizondo, E.; Esteban, O.; Corchero, J. L.; Melgarejo, M.; Pulido, D.; Córdoba, A.; Moreno, E.; Unzueta, U.; Vazquez, E.; Abasolo, I.; Schwartz, S.; Villaverde, A.; Albericio, F.; Royo, M.; García-Parajo, M. F.; Ventosa, N.; Veciana, J. Multifunctional Nanovesicle-Bioactive Conjugates Prepared by a One-Step Scalable Method Using CO2-Expanded Solvents. *Nano Lett.* **2013**, *13*, 3766−3774.
(25) Vargas-Nadal, G.; Muñoz-Ubeda, M.; Alamo, P.; Arnal, M. M.; Céspedes, V.; Köber, M.; Gonzalez, E.; Ferrer-Tasies, L.; Vinardell, M. P.; Mangues, R.; Veciana, J.; Ventosa, N. MKC-Quatsomes: A Stable Nanovesicle Platform for Bio-Imaging and Drug-Delivery Applications. *Nanomedicine* **2019**, No. 102136.
(26) Segura Ginard, F. M.; Gallego Melcon, S.; Sánchez de Toledo Codina, J.; Soriano Fernánez, A.; Ventosa Rull, N.; Veciana Miró, J.; Boloix Amenós, A.; Segovia Ramos, N. V. Nanovesicles and Its Use for Nucleic Acid Delivery. E. P. Patent EP193823722019.
(27) Ardizzone, A.; Blasi, D.; Vona, D.; Rosspeintner, A.; Punzi, A.; Altamura, E.; Grimaldi, N.; Sala, S.; Vauthey, E.; Farinola, G. M.; Ratera, I.; Ventosa, N.; Veciana, J. Highly Stable and Red-Emitting Nanovesicles Incorporating Lipophilic Diketopyrrolopyrroles for Cell Imaging. *Chem. - Eur. J.* **2018**, *24*, 11386−11392.
(28) Ardizzone, A.; Kurhuzenkau, S.; Illa-Tuset, S.; Faraudo, J.; Bondar, M.; Hagan, D.; Van Stryland, E. W.; Painelli, A.; Sissa, C.; Feiner, N.; Albertazzi, L.; Veciana, J.; Ventosa, N. Nanostructuring Lipophilic Dyes in Water Using Stable Vesicles, Quatsomes, as Scaffolds and Their Use as Probes for Bioimaging. *Small* **2018**, *14*, No. 1703851.

(29) Iqbal, A.; Arslan, S.; Okumus, B.; Wilson, T. J.; Giraud, G.; Norman, D. G.; Ha, T.; Lilley, D. M. J. Orientation Dependence in Fluorescent Energy Transfer between Cy3 and Cy5 Terminally Attached to Double-Stranded Nucleic Acids. *Proc. Natl. Acad. Sci. U. S. A.* **2008**, *105*, 11176−11181.
(30) Elizondo, E.; Larsen, J.; Hatzakis, N. S.; Cabrera, I.; Bjørnholm, T.; Veciana, J.; Stamou, D.; Ventosa, N. Influence of the Preparation Route on the Supramolecular Organization of Lipids in a Vesicular System. *J. Am. Chem. Soc.* **2012**, *134*, 1918−1921.
(31) Bozzuto, G.; Molinari, A. Liposomes as Nanomedical Devices. *Int. J. Nanomed.* **2015**, *10*, 975−999.
(32) Mishra, A.; Behera, R. K.; Behera, P. K.; Mishra, B. K.; Behera, G. B. Cyanines during the 1990s: A Review. *Chem. Rev.* **2000**, *100*, 1973−2012.
(33) Gadde, S.; Batchelor, E. K.; Kaifer, A. E. Controlling the Formation of Cyanine Dye H- and J-Aggregates with Cucurbituril Hosts in the Presence of Anionic Polyelectrolytes. *Chem. - Eur. J.* **2009**, *15*, 6025−6031.
(34) Berlepsch, H. v.; Böttcher, C. H-Aggregates of an Indocyanine Cy5 Dye: Transition from Strong to Weak Molecular Coupling. *J. Phys. Chem. B* **2015**, *119*, 11900−11909.
(35) Sanborn, M. E.; Connolly, B. K.; Gurunathan, K.; Levitus, M. Fluorescence Properties and Photophysics of the Sulfoindocyanine Cy3 Linked Covalently to DNA. *J. Phys. Chem. B* **2007**, *111*, 11064−11074.
(36) Packard, B. S.; Wolf, D. E. Fluorescence Lifetimes of Carbocyanine Lipid Analogs in Phospholipid Bilayers. *Biochemistry* **1985**, *24*, 5176−5181.
(37) Gumí-Audenis, B.; Illa-Tuset, S.; Grimaldi, N.; Pasquina-Lemonche, L.; Ferrer-Tasies, L.; Sanz, F.; Veciana, J.; Ratera, I.; Faraudo, J.; Ventosa, N.; Giannotti, M. I. Insights into the Structure and Nanomechanics of a Quatsome Membrane by Force Spectroscopy Measurements and Molecular Simulations. *Nanoscale* **2018**, *10*, 23001−23011.
(38) Mujumdar, R. B.; Ernst, L. A.; Mujumdar, S. R.; Lewis, C. J.; Waggoner, A. S. Cyanine Dye Labeling Reagents: Sulfoindocyanine Succinimidyl Esters. *Bioconjugate Chem.* **1993**, *4*, 105−111.
(39) Klehs, K.; Spahn, C.; Endesfelder, U.; Lee, S. F.; Fürstenberg, A.; Heilemann, M. Increasing the Brightness of Cyanine Fluorophores for Single-Molecule and Superresolution Imaging. *ChemPhysChem* **2014**, *15*, 637−641.
(40) Benson, R. C.; Kues, H. A. Absorption and Fluorescence Properties of Cyanine Dyes. *J. Chem. Eng. Data* **1977**, *22*, 379−383.
(41) Lim, S. J.; Zahid, M. U.; Le, P.; Ma, L.; Entenberg, D.; Harney, A. S.; Condeelis, J.; Smith, A. M. Brightness-Equalized Quantum Dots. *Nat. Commun.* **2015**, *6*, No. 8210.
(42) Corredor, C. C.; Belfield, K. D.; Bondar, M. V.; Przhonska, O. V.; Yao, S. One- and Two-Photon Photochemical Stability of Linear and Branched Fluorene Derivatives. *J. Photochem. Photobiol., A* **2006**, *184*, 105−112.
(43) Ahn, H.-Y.; Yao, S.; Wang, X.; Belfield, K. D. Near-Infrared-Emitting Squaraine Dyes with High 2PA Cross-Sections for Multiphoton Fluorescence Imaging. *ACS Appl. Mater. Interfaces* **2012**, *4*, 2847−2854.
(44) Mustroph, H.; Reiner, K.; Mistol, J.; Ernst, S.; Keil, D.; Hennig, L. Relationship between the Molecular Structure of Cyanine Dyes and the Vibrational Fine Structure of Their Electronic Absorption Spectra. *ChemPhysChem* **2009**, *10*, 835−840.
(45) Basu, S.; Needham, L.-M.; Lando, D.; Taylor, E. J. R.; Wohlfahrt, K. J.; Shah, D.; Boucher, W.; Tan, Y. L.; Bates, L. E.; Tkachenko, O.; Cramard, J.; Lagerholm, B. C.; Eggeling, C.; Hendrich, B.; Klenerman, D.; Lee, S. F.; Laue, E. D. FRET-Enhanced Photostability Allows Improved Single-Molecule Tracking of Proteins and Protein Complexes in Live Mammalian Cells. *Nat. Commun.* **2018**, *9*, No. 2520.
(46) Liu, X.; Ardizzone, A.; Sui, B.; Anzola, M.; Ventosa, N.; Liu, T.; Veciana, J.; Belfield, K. D. Fluorenyl-Loaded Quatsome Nanostructured Fluorescent Probes. *ACS Omega* **2017**, *2*, 4112−4122.
(47) Melnychuk, N.; Egloff, S.; Runser, A.; Reisch, A.; Klymchenko, A. S. Light-Harvesting Nanoparticle Probes for FRET-Based Detection of Oligonucleotides with Single-Molecule Sensitivity. *Angew. Chem., Int. Ed.* **2020**, *132*, 6878−6885.
(48) Scaiano, J. C. *Handbook of Organic Photochemistry*; CRC Press, 1989.
(49) Strickler, S. J.; Berg, R. A. Relationship between Absorption Intensity and Fluorescence Lifetime of Molecules. *J. Chem. Phys.* **1962**, *37*, 814−822.
(50) Belfield, K. D.; Bondar, M. V.; Przhonska, O. V.; Schafer, K. J. Photochemical Properties of (7-Benzothiazol-2-Yl-9,9-Didecylfluoren-2-Yl)Diphenylamine under One- and Two-Photon Excitation. *J. Photochem. Photobiol., A* **2004**, *162*, 569−574.
(51) Belfield, K. D.; Bondar, M. V.; Liu, Y.; Przhonska, O. V. Photophysical and Photochemical Properties of 5,7-Dimethoxycoumarin under One- and Two-Photon Excitation. *J. Phys. Org. Chem.* **2003**, *16*, 69−78.
(52) Valeur, B. B.; Nuno, M. Effects of Intermolecular Photophysical Processes on Fluorescence Emission. *Mol. Fluoresc.* **May 3, 2012**, 141−179.

https://dx.doi.org/10.1021/acsami.0c03040
ACS Appl. Mater. Interfaces 2020, 12, 20253−20262